Ultrasensitive, fast, thin-film differential scanning calorimeter

Mikhail Yu. Efremov, Eric A. Olson, Ming Zhang, François Schiettekatte, Zishu Zhang, and Leslie H. Allen[a)]
Department of Materials Science and Engineering and the Coordinated Science Laboratory, University of Illinois at Urbana–Champaign, Urbana, Illinois 61801

(Received 1 July 2003; accepted 12 October 2003)

The equipment for an ultrasensitive, fast, thin-film differential scanning calorimetry [(TDSC) or nanocalorimetry] technique is described. The calorimetric cell (~0.30 cm^2) operates by applying a short (~10 ms) dc current pulse (~10 mA) to a thin (~50 nm) patterned metal strip, which is supported by a thin (~50 nm) SiN_x membrane. The calorimeter operates at high heating rates (15–200 K/ms) and is very sensitive (30 pJ/K). The design of the calorimeter, the timing/synchronization methods, as well as the choice of key components of the instrument are discussed. Comparisons are made between two dc pulsing circuits that generate the current, a battery powered system and a system based on discharge of an assembly of charged capacitors (recommended). Design concepts for the differential as well as a simplified nondifferential technique are discussed and evaluated via experiments on thin films of indium. The differential design shows an increase in sensitivity, making it suitable for small samples. The custom made electronic circuits are also described, including the design of a preamplifier with low (28×) and high (700×) gain options, which are also compared using experimental data. Noise considerations are critical for the method. Simple models which describe noise levels in the calorimetric data are given and methods for reducing noise are discussed in detail. The sources of noise in the instrument are discussed in terms of both fundamental factors such as Johnson noise of the metal strip, as well as the limiting attributes of the sensing and pulsing circuits and instrumentation. These limiting attributes include spurious signals generated by desorption of ambient gases from the sensor, ground loops, switching regulators, and missing codes in analog-to-digital converter instruments. Examples of the experimental data of heat capacity $Cp(T)$ of various thin films of indium, tin, and polystyrene are presented. A complete data set of raw experimental values is included for a 20 nm sample of Sn which shows the values of current and voltage of both the sample and reference sensors, as well as the differential voltage and the final values of the heat capacity. © *2004 American Institute of Physics.* [DOI: 10.1063/1.1633000]

I. INTRODUCTION

Thin-film differential scanning calorimetry [(TDSC), or nanocalorimetry] is a technique by which to probe the thermophysical properties of films with nanometer-scale thickness. TDSC has been used in investigations of the melting properties of small (down to 2 nm diameter) supported particles of In, Sn, and Al (Refs. 1–3, and references therein), microscopic monocrystals of polyethylene,[4] and glass transition in 1–400 nm thick films of polystyrene, poly(2-vinyl pyridine), and poly(methyl methacrylate) (Ref. 5 and references therein). Similar methods have been discussed[6] and used to study melting and crystallization in linear polyethylene.[7] Fabrication of the microelectromechanical system (MEMS)-based sensor (calorimetro cell) and basic data processing are described elsewhere.[8,9] Here we discuss in detail the equipment needed for the nanocalorimetry technique and the hardware-introduced uncertainties of this method.

II. PRINCIPLES OF OPERATION

The TDSC sensors are fabricated by a standard microlithographic process on Si wafers. The sensor consists of an extremely thin (30–400 nm thick) SiN_x membrane supported by a Si frame, as illustrated in Fig. 1 (top plot). The lateral dimensions of the membrane are several millimeters. A thin (typically 50 nm thick) metal strip is fabricated on the top of the sensor across the membrane. The typical width of the strip is 0.5 mm. Fabrication of the TDSC sensors is discussed in detail elsewhere.[8] Figure 1 (bottom plot) gives a brief schematic of the microfabrication process.

The sample investigated is deposited either directly onto the metal strip or onto the SiN_x side beneath the strip. During operation (calorimetric *scan*), a pulse of current is applied through the metal strip. The strip serves both as a heater and as a thermometer. Only the part of the strip placed on the membrane far from the Si frame can be heated effectively. Metallization on the frame remains cold due to the high heat capacity of thick (typically 0.25 mm) and massive (in comparison with the membrane) Si frame. The temperature of the center (working) part of the heater on the membrane can be measured by its resistance. To do this, the voltage across the working part of heater V is monitored during the scan via patterned electrical probes (see Fig. 1). Using the value of current I through the heater, also monitored during the experiment, resistance R and temperature T as functions of time t can be calculated. The simplified circuitry used for this

a)Electronic mail: L-ALLEN9@uiuc.edu

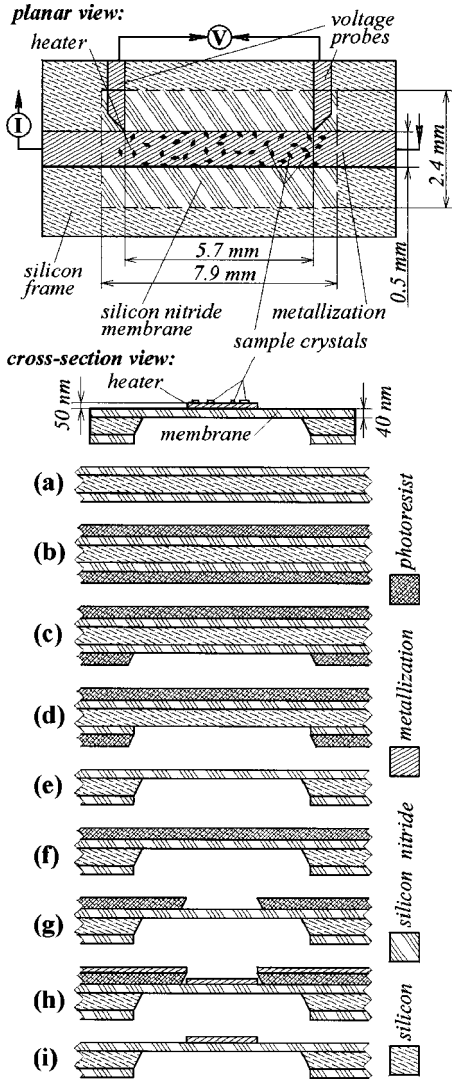

FIG. 1. Top plot: Planar and cross-sectional views of a typical TDSC sensor with a sample on it (not to scale). Bottom plot: Cross-sectional view of the sensor at nine points during microfabrication. (a) Low stress SiN_x is deposited on both sides of a wafer using low pressure chemical vapor deposition. (b) Both sides of a wafer are coated with photoresist. (c) A photoresist layer is patterned and developed. (d) A section of the SiN_x is etched away by reactive ion etching. (e) The photoresist is removed and the exposed Si is etched in an alkaline solution. (f) A photoresist layer is spun onto the front side of the wafer. (g) The photoresist layer is patterned, the tone of the exposure is reversed, and the photoresist layer is developed. (h) A metal layer is deposited on the front side of the wafer. (i) The finished wafer after a lift-off procedure.

measurement is illustrated in Fig. 2. The $R(T)$ function should be evaluated by a calibration procedure prior to the experiment.

The working part of the heater, the sample on it (if any), and the part of SiN_x beneath it form a calorimetric *cell*. Using high current, it is possible to approach adiabatic working conditions, since the extremely fast heating rate provides no time for dissipation of the heat from the cell to its surroundings. In this case, all Joule heat, with power $P=IV$ generated by the heater, is consumed by an increase in the temperature of the cell:

$$P(t)dt = C_P(T)dT, \tag{1}$$

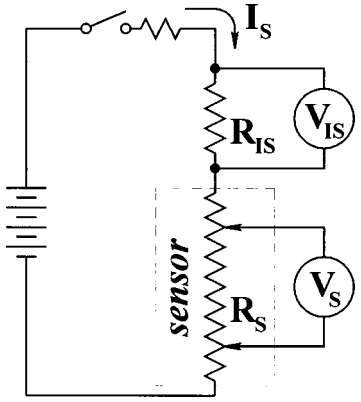

FIG. 2. Nondifferential scheme of TDSC.

where $C_P(T)$ is the total heat capacity of the cell. $C_P(T)$ is the sum of the heat capacity of the empty cell (*addenda*) $C_P^{\text{cell}}(T)$, which can be measured in a separate (idle) experiment, and the heat capacity of the sample $C_P^{\text{SMP}}(T)$.

The remarkably low thickness of the cell constituents, i.e., the heater and the membrane, provides an extremely small addenda, which is key to high sensitivity of the TDSC method. However, this characteristic of the sensor in itself is not enough to achieve the sensitivity demonstrated.[1] The *differential* scheme greatly improves the measurement. Two sensors are used in this case, one with sample material on it (the *sample* sensor) and the other without (the *reference* sensor), as illustrated in Fig. 3. During a scan, synchronized pulses of current from two separate supplies are applied to the sensors. Figure 4 shows an example of typical raw experimental data. Current through the heaters I_S and I_R [Fig. 4(a)], voltage across the heaters V_S and V_R [Fig. 4(b)], and differential voltage ΔV [Fig. 4(e)] are monitored during the experiment (where indices S and R are the sample and reference sensors, respectively). It has been shown,[9] that the useful signal, i.e., the heat capacity of the sample, is roughly proportional to the derivative of ΔV over time [demonstrated in Fig. 4(e)]: $C_P^{\text{SMP}} \propto d\Delta V/dt$. The I_S, I_R, V_S, and V_R data are used to calculate the resistance of heaters R_S and R_R [shown in Fig. 4(c)] and temperature of calorimetric cells T_S and T_R [Fig. 4(d)]. The final output, the heat capacity of sample C_P^{SMP} as a function of sample temperature T_S (calorimetric curve), is shown in Fig. 4(f).

Typical experimental parameters are as follows. The heating rates are from 15 to 200 K/ms. The scanning temperature interval is from room temperature to 300 °C; this corresponds to 1.5–20 ms scan time. For the typical heat capacity of an empty cell of 500–1000 nJ/K and resistance

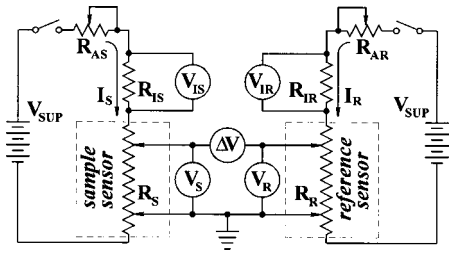

FIG. 3. Differential scheme of TDSC.

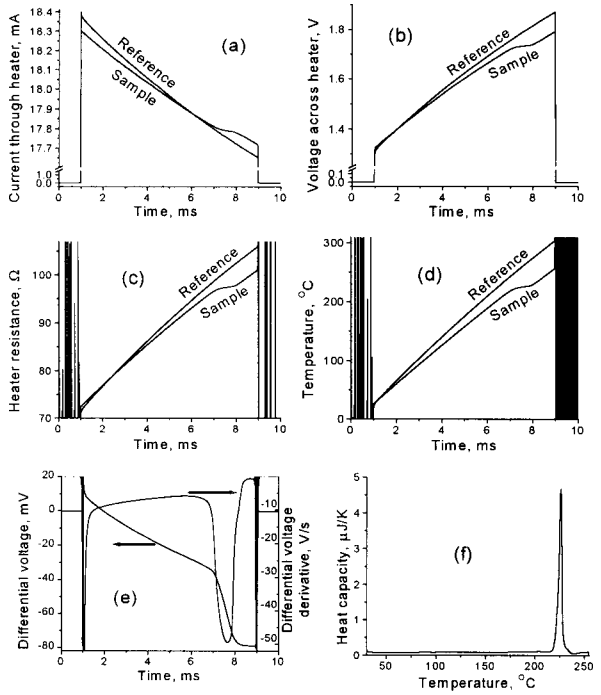

FIG. 4. (a)–(e) Raw experimental data and (f) final result for TDSC measurement of the 20 nm Sn film deposited on the sensor with Pt metallization. A current pulse of 8 ms duration starts at 1 ms. (a) Current through the heaters, (b) voltage across them, (c) heater resistance and (d) temperature for both the sample and reference sensors. Data for resistance and temperature are not valid when there is no current applied (<1 ms and >9 ms). (e) Differential voltage and its derivative over time; (f) the final $C_P(T)$ curve of the sample.

of 50–150 Ω (for a Pt heater), the current through the heater is 10–50 mA and the voltage across it is 1–5 V. To get temperature resolution of about 1 K per reading, all electrical parameters are typically measured at a sampling rate of 100 ksamples/s (100 kHz).

III. DSC EQUIPMENT

A. Error analysis: Nondifferential mode

To analyze hardware requirements in the case of the nondifferential variant of the TDSC method, we will express errors in sample heat capacity using distributions of experimentally measured values of V_{IS} and V_S (see Fig. 2). Let us assume that the values of voltage measurement have random normally distributed deviations. We characterize these deviations in the voltage data by the root-mean-square (rms) value of deviation ε_V, which we refer to as the voltage *error* or *noise*. Let ε_{VIS} and ε_{VS} be voltage errors (noise) of V_{IS} and V_S, respectively. According to Eq. (1), the heat capacity of the cell is found to be

$$C_P = \frac{P}{dT/dt}. \tag{2}$$

The term with the most noise, dT/dt, is calculated using $R_S(t)$, which, in turn, is calculated from V_{IS} and V_S. Using the relationship

$$\frac{1}{R_S}\frac{dR_S}{dt} = \alpha\frac{dT}{dt}, \tag{3}$$

where α is the temperature coefficient of the resistivity, and noting from the circuit in Fig. 2 that

$$I_S = \frac{V_S}{R_S} = \frac{V_{IS}}{R_{IS}}, \tag{4}$$

the dT/dt term can be expressed as

$$\frac{dT}{dt} = \frac{1}{\alpha R_S}\frac{d[R_{IS}(V_S/V_{IS})]}{dt} = \frac{1}{\alpha V_S}\frac{dV_S}{dt} - \frac{1}{\alpha V_{IS}}\frac{dV_{IS}}{dt}. \tag{5}$$

Numerically, for both V_{IS} and V_S, the derivative dV/dt is expressed as $(V_{i+1}-V_i)/\Delta t$, where V_i and V_{i+1} are consecutive data points of voltage measurements and Δt is the reciprocal of sampling frequency f_S:

$$\Delta t = \frac{1}{f_S}. \tag{6}$$

Therefore, for the derivatives dV_{IS}/dt and dV_S/dt, the errors (noise) are $\sqrt{2}\varepsilon_{VIS}/\Delta t$ and $\sqrt{2}\varepsilon_{VS}/\Delta t$, respectively. The error (noise) of dT/dt ($\varepsilon_{dT/dt}$) can be expressed via the errors of two terms in Eq. (5):

$$\varepsilon_{dT/dt}^2 = \frac{2\varepsilon_{VS}^2}{\alpha^2 V_S^2(\Delta t)^2} + \frac{2\varepsilon_{VIS}^2}{\alpha^2 V_{IS}^2(\Delta t)^2} = \frac{2\varepsilon_{VS}^2}{\alpha^2 V_S^2(\Delta t)^2}\left[1+\left(\frac{\varepsilon_{VIS}}{\varepsilon_{VS}}\frac{R_S}{R_{IS}}\right)^2\right] \tag{7}$$

[for the last transformation we use Eq. (4)]. The fractional error of $C_P(\delta_{Cp})$, which is practically equal to the fractional error of the derivative dT/dt ($\delta_{dT/dt}$), can be expressed using Eq. (7):

$$\delta_{Cp} \approx \delta_{dT/dt} = \frac{\sqrt{2}\varepsilon_{VS}}{\alpha V_S \Delta t\left(\frac{dT}{dt}\right)}\sqrt{1+\left(\frac{\varepsilon_{VIS}}{\varepsilon_{VS}}\frac{R_S}{R_{IS}}\right)^2}. \tag{8}$$

Values V_S and dT/dt are mutually dependent. Using the formula $P = V_S^2/R_S$ and Eq. (2), we can express V_S as

$$V_S = \sqrt{R_S C_P \frac{dT}{dt}}. \tag{9}$$

The value of *temperature resolution* r_T for a TDSC scan can be determined as a difference in temperature for two consecutive readings:

$$r_T = \Delta t\frac{dT}{dt}. \tag{10}$$

For simplicity, we assume that the heat capacity of sample C_P^{SMP} is much less than the heat capacity of the cell itself: $C_P^{\mathrm{SMP}} \ll C_P$. This is also the most interesting case, because when C_P^{SMP} is comparable with the addenda or even larger, the signal is strong enough to be much larger than the noise in experimental output.

In order to obtain C_P^{SMP}, the heat capacity of cell C_P should be measured twice (both with and without the sample). Then, by combining Eqs. (6) and (8)–(10) the fractional error of $C_P^{\mathrm{SMP}}(\delta_{Cp\mathrm{SMP}})$ can be approximated by

$$\delta_{Cp\mathrm{SMP}} \approx \sqrt{2}\,\frac{\delta_{Cp} C_P}{C_P^{\mathrm{SMP}}} = \frac{2\varepsilon_{VS}\sqrt{C_P}}{\alpha r_T^{3/2} C_P^{\mathrm{SMP}} \sqrt{R_S f_S}} \sqrt{1+\left(\frac{\varepsilon_{VIS}}{\varepsilon_{VS}}\frac{R_S}{R_{IS}}\right)^2}. \quad (11)$$

Note that the heat capacities in the last equation can be easily estimated using the following formulas:

$$C_P = lw(c_{\mathrm{Me}}\rho_{\mathrm{Me}}h_{\mathrm{Me}} + c_{\mathrm{SiN}}\rho_{\mathrm{SiN}}h_{\mathrm{SiN}}) \quad (12)$$

and

$$C_P^{\mathrm{SMP}} = lwc_{\mathrm{SMP}}\rho_{\mathrm{SMP}}h_{\mathrm{SMP}}, \quad (13)$$

where c is specific heat capacity, ρ is the specific density, h is the thickness, l is the distance between two voltage probes, w is the width of the heater strip, and indices Me, SiN, and SMP denote metal of the metallization layer, SiN_x, and the sample, respectively. Parameter h_{SMP} has a special meaning of the *average* sample thickness if the sample is a discontinuous film or does not cover the working part of the heater entirely.

According to Eq. (11), minimization of voltage noise ε_V (both ε_{VS} and ε_{VIS}) is crucial for sensitivity in a nondifferential calorimetric experiment. The value of ε_V is an important metrologic characteristic which can typically be found in documentation of voltmeters [or analog-to-digital converters (ADCs)]. ε_V depends on the regime of the voltmeter: the range, sampling rate, etc. A properly chosen range can sufficiently decrease measurement error. Generally, ε_V is reduced by narrowing the measurement range, either by decreasing the range of amplitude, or changing from bipolar to unipolar mode. Unipolar mode can be used because both V_{IS} and V_S are unipolar.

According to Eq. (11) (the last radical term), increasing of the value of current measurement resistor R_{IS} can also improve noise characteristics. Some limitations of this method are discussed in Sec. III G3. Note that increasing R_{IS} can also lead to an increase in the range of its corresponding ADC and, subsequently, to an increase in noise ε_{VIS}. In a properly optimized system, the last radical term in Eq. (11) would be close to unity so a simplified expression for $\delta_{Cp\mathrm{SMP}}$ can be used:

$$\delta_{Cp\mathrm{SMP}} \approx \frac{2\sqrt{C_P}}{\alpha r_T^{3/2} C_P^{\mathrm{SMP}} \sqrt{R_S f_S}}\,\varepsilon_{VS}. \quad (14)$$

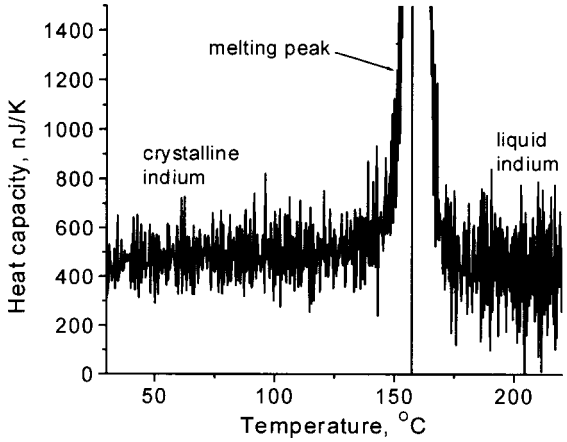

FIG. 5. Calorimetric curve obtained by nondifferential mode TDSC. The curve is an average of 100 scans. Sample: 100 nm thick indium deposit. Parameters for error estimation (close to room temperature): ADCs: $\varepsilon_{VIS}=80\ \mu$V, $\varepsilon_{VS}=120\ \mu$V. $R_{IS}=20\ \Omega$. Sensor with platinum metallization, $\alpha=0.0019\ \mathrm{K}^{-1}$, $R_S=70\ \Omega$. $C_P=0.65\ \mu$J/K, heating rate 35 K/ms.

Figure 5 illustrates a calorimetric curve obtained by the nondifferential method. Using Eq. (11) and the experimental parameters in the caption of Fig. 5 ($\varepsilon_{VIS}=80\ \mu$V, $\varepsilon_{VS}=120\ \mu$V, $R_{IS}=20\ \Omega$, $R_S=70\ \Omega$, $\alpha=0.0019\ \mathrm{K}^{-1}$, $C_P=650$ nJ/K, $C_P^{\mathrm{SMP}}=450$ nJ/K, $f_S=100$ kHz, $dT/dt=35$ K/ms, number of scans -100) we can estimate

$$\delta_{Cp\mathrm{SMP}}\big|_{\mathrm{R.T.}} \approx \frac{1}{\sqrt{100\ \text{scans}}} \times \frac{2\times\sqrt{650\ \text{nJ/K}}\times 120\ \mu\text{V}\times\sqrt{1+[(80\ \mu\text{V}/120\ \mu\text{V})\times(70\ \Omega/20\ \Omega)]^2}}{0.0019\ \text{K}^{-1}\times(35\ \text{K/ms}/100\ \text{kHz})^{3/2}\times\sqrt{70\ \Omega\times 100\ \text{kHz}}\times 450\ \text{nJ/K}} = 0.10.$$

For comparison with Fig. 5, the peak-to-peak value of the absolute error at room temperature (RT) can be estimated as $0.10\times 450\ \text{nJ/K}\times 6 \approx 300\ \text{nJ/K}$, which is in excellent agreement with the data presented in Fig. 5.

B. Error analysis: Differential mode

For analysis of noise in differential mode (see the scheme in Fig. 3), let us start with an approximate equation,[9]

$$C_P^{\mathrm{SMP}} \approx -\frac{V_R}{\alpha_R R_R (dT_R/dt)^2}\times\frac{d\Delta V}{dt}. \quad (15)$$

Index R denotes the reference sensor or circuit. The derivative of differential voltage ΔV over time t is typically the term with most noise in Eq. (15). As in Sec. III A, we assume that the noise of ΔV is random and normally distributed, and characterize it by the rms value of deviations, voltage error $\varepsilon_{\Delta V}$. Similar to in Sec. III A, the error of $d\Delta V/dt$ is $\sqrt{2}\varepsilon_{\Delta V}/\Delta t$. Since the fractional error of C_P^{SMP} ($\delta_{Cp\mathrm{SMP}}$) is close to the fractional error of $d\Delta V/dt$, one finds that

$$\delta_{Cp\mathrm{SMP}} \approx \frac{2V_R\varepsilon_{\Delta V}}{\alpha_R R_R \Delta t (dT_R/dt)^2 C_P^{\mathrm{SMP}}}. \quad (16)$$

Note that an additional $\sqrt{2}$ coefficient is added to Eq. (16) because two heat capacity measurements are required to obtain C_P^{SMP} (one with and one without the sample). V_R and dT_R/dt are mutually dependent. As in Sec. III A, combination of Eqs. (6), (9), (10), and (16) gives

$$\delta_{Cp\mathrm{SMP}} \approx \frac{2\sqrt{C_P}}{\alpha r_T^{3/2} C_P^{\mathrm{SMP}} \sqrt{R_S f_S}} \varepsilon_{\Delta V}. \tag{17}$$

Here we assume that α and the resistance of both the sample and reference sensors are the same.

Figure 6 illustrates the calorimetric curve obtained by the differential method. Using Eq. (17) and the experimental parameters in the caption of Fig. 6 ($\varepsilon_{\Delta V}=500\ \mu$V, $R_S=70\ \Omega$, $\alpha=0.0019\ \mathrm{K}^{-1}$, $C_P=650$ nJ/K, $C_P^{\mathrm{SMP}}=13$ nJ/K, $f_S=100$ kHz, $dT/dt=40$ K/ms, number of scans -100, gain of the preamplifier $g=-28$) we can estimate

$$\delta_{Cp\mathrm{SMP}}|_{\mathrm{R.T.}} \approx \frac{1}{\sqrt{100\ \text{scans}}} \times \frac{2\times\sqrt{650\ \text{nJ/K}}\times 500\ \mu\text{V}/|-28|}{0.0019\ \text{K}^{-1}\times(40\ \text{K/ms}/100\ \text{kHz})^{3/2}\times\sqrt{70\ \Omega\times 100\ \text{kHz}}\times 13\ \text{nJ/K}} = 0.17,$$

where 13 nJ/K is roughly the heat capacity of the sample close to room temperature. For comparison with Fig. 6, the peak-to-peak value of the absolute error at room temperature can be estimated to be $0.17\times 13\ \text{nJ/K}\times 6\approx 13$ nJ/K, which is in excellent agreement with the data presented in Fig. 6.

Note that, in comparison with the nondifferential measurement in Fig. 5, the differential measurement in this example gives about (300 nJ/K)/(13 nJ/K)≈20-fold improvement in the noise level. Other parameters of these two measurements are close to each other, except that of the noise characteristics of the ADC for ΔV measurements (ΔV–ADC), which are even worse than those of the ADCs used in the nondifferential experiment in shown in Fig. 5.

The nature of the demonstrated advantage of the differential method becomes clear if we compare expressions for fractional errors in nondifferential ($\delta_{Cp\mathrm{SMP}}^{\mathrm{nondif}}$) and differential ($\delta_{Cp\mathrm{SMP}}^{\mathrm{dif}}$) methods [see Eqs. (14) and (17)]:

$$\frac{\delta_{Cp\mathrm{SMP}}^{\mathrm{nondif}}}{\delta_{Cp\mathrm{SMP}}^{\mathrm{dif}}} = \frac{\varepsilon_{VS}}{\varepsilon_{\Delta V}}. \tag{18}$$

For small samples, the measured differential signal ΔV is close to zero. Consequently, the ΔV–ADC range of measurement can be effectively reduced, which causes a large reduction in the noise level $\varepsilon_{\Delta V}$ (see the note about choosing the range of measurement in Sec. III A). In most cases, the simplest method for reducing the ΔV–ADC range is using a preamplifier with an absolute value of gain $|g|>1$ and negligible noise. In this case, the effective noise of ΔV–ADC would be smaller than the specified value by factor of $|g|$. That is, a preamplifier with gain $g=-28$ makes $\delta_{Cp\mathrm{SMP}}$ for a differential measurement (in the example above) much smaller than for a nondifferential one.

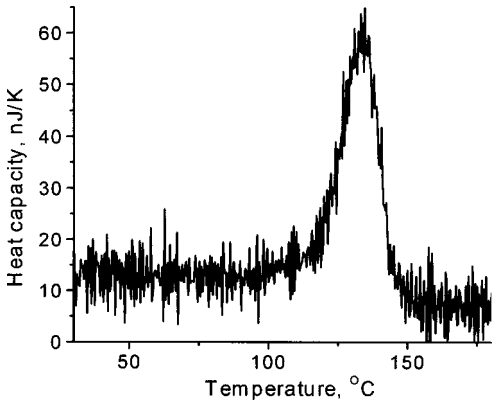

FIG. 6. Calorimetric curve obtained by regular (differential) mode TDSC. The curve is an average of 100 scans. Sample: 2 nm thick indium deposit. Parameters for error estimation (close to room temperature): ΔV–ADC: $\varepsilon_{\Delta V}=500\ \mu$V, 100 kHz sampling rate, with preamplifier, gain $g=-28$. Sensor with platinum metallization, $\alpha=0.0019\ \mathrm{K}^{-1}$, $C_P=0.65\ \mu$J/K, heating rate 40 K/ms. $R_S=70\ \Omega$.

However, it should be noted that decreasing the noise of ΔV–ADC by using preamplifiers with large gain has limitations. Since, in practice, ΔV is not exactly zero even for infinitesimal samples, using large gains would lead to overrange conditions. Additionally, some types of noise in the TDSC assembly (i.e., noise of the current supply, thermal noise of the sensors, internal noise of the preamplifier) scale with the gain of the preamplifier and become a dominant factor at large enough gains. These issues are discussed in detail in Secs. III E–III G.

A related problem is the choice between differential and nondifferential modes of operation for the given sample. For samples with heat capacities much smaller than the addenda ($C_P^{\mathrm{SMP}} \ll C_P^{\mathrm{cell}}$), differential mode usually is the only choice. However, when C_P^{SMP} is comparable with C_P^{cell} or larger (for simplicity, average thicknesses of the sample and the working part of sensor can be compared instead of heat capacities), the signal will be large enough to make using the nondifferential mode feasible. In this case of a strong signal, the gain of the preamplifier should be small enough to prevent overrange conditions. However, with a decrease in gain, the difference in sensitivity between two modes vanishes, and a technically more simple nondifferential mode can be more favorable.

C. Error analysis: Additional considerations

The following considerations are applicable both for nondifferential and differential modes of TDSC.

Noise $\delta_{Cp\mathrm{SMP}}$ can also be effectively reduced at the expense of the temperature resolution, r_T: $\delta_{Cp\mathrm{SMP}} \propto r_T^{-3/2}$ [see Eqs. (11) and (17)]. It is worth noting that simple box averaging (smoothing) of the $C_P(T)$ curve is not effective, because any improvement in noise would be proportional only to $r_T^{-1/2}$. A more detailed discussion can be found elsewhere.[9]

Averaging of more than one scans is an effective and practical way to reduce the noise. Generally, $\delta_{Cp\mathrm{SMP}}$

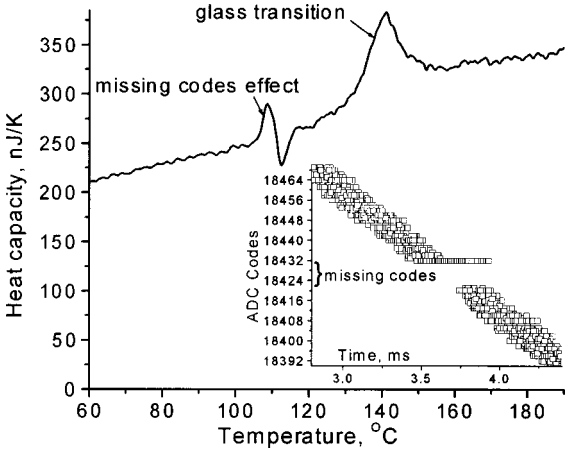

FIG. 7. Effect of missing codes. Heat capacity vs temperature curve for 55 nm thick spin-cast polystyrene film. Voltages V_{IS} and V_{IR} are measured using ADCs with missing codes. Inset: ADC output codes for the V_{IS} value vs the time of scan. Note that missing codes are of the type $N\times 2^M$, where N and M are integers (in this example, $18\,432=9\times 2^{11}$).

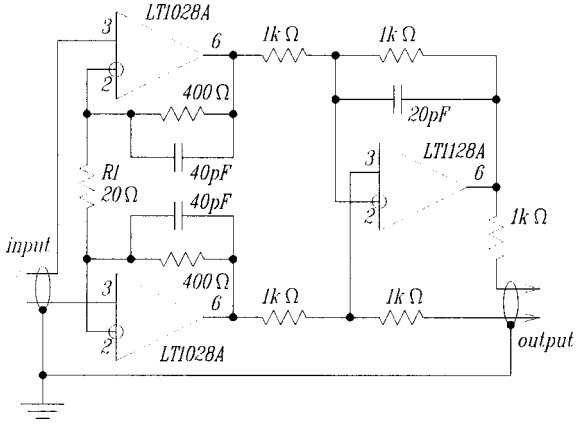

FIG. 8. Schematic electrical diagram of the preamplifier. All resistors are 1% wire wound (preferred) or metal film type, and capacitors are mica or polystyrene type. Gain g can be easily varied by resistor $R1$. In the configuration shown, $g=-41$.

$\propto 1/\sqrt{N}$, where N is the number of scans to be averaged. However, there are limitations to this method. First, time is of concern. For example, 100-fold improvement would take about 3 h of scanning (10 000 s) with a typical time of 1 s between consecutive scans. Second, only repeatable scans can be averaged. Irreversible processes such as decomposition, coalescence, desorption, etc. should be recorded by a single scan. Third, averaging assumes *random* noise. Generally, all voltmeters are characterized by some level of *spurious signals*, which are not random and will not vanish during averaging. The extreme example of the spurious signal is the *missing codes effect*, when the transfer function of the ADC is so nonlinear that some codes cannot be reached at any input value of voltage. The example of TDSC measurement, where the V_{IS} voltmeter has missing codes, is shown in Fig. 7.

Using the methods of noise suppression discussed above, it is possible to increase the resolution of the heat capacity measurement to 30 pJ/K (or better), which is equivalent to resolution of 0.04 Å of average thickness of deposited indium film.[3]

D. ADCs used in TDSC: Additional considerations

Most ADCs, which can serve as $\Delta V-$ADCs, can work also as ADCs for V_{IS}, V_{IR}, V_S, and V_R measurements. However, TDSC optimization makes different demands for $\Delta V-$ADC and ADCs for nondifferential (ND-ADCs) parameters.

Good dc characteristics are more important for ND-ADCs. Calorimetric cell temperature T is the most sensitive parameter for errors such as significant offset, gain error, and integral nonlinearity. Using Eqs. (3) and (4), the error of $T(\varepsilon_T)$ is found to be

$$\varepsilon_T=\frac{1}{\alpha}\sqrt{\delta_{VS}^2+\delta_{VIS}^2}, \tag{19}$$

where δ_{VS} and δ_{VIS} are fractional errors of V_S and V_{IS}. Due to small values of α, ε_T is sensitive to δ_{VS} and δ_{VIS}. For example, $\delta_{VS}=\delta_{VIS}=0.1\%$ (*accuracy* of 0.1% is not a bad value for ADCs with 100 kHz sampling frequency) and $\alpha=0.0019\ \mathrm{K}^{-1}$ (from the examples discussed above) give $\varepsilon_T\approx 0.7$ K, which cannot be intolerated in some precise experiments.

In contrast, ΔV measurements are resistant to dc errors such as offset and gain error. Since C_P is proportional to the ΔV derivative [Eq. (15)], the offset has no importance. Gain error would proportionally magnify the C_P value; since error in the absolute C_P value of a few percent is typically acceptable, gain error is not very important either.

The ac characteristics are very important for both ND-ADCs and $\Delta V-$ADC, but the latter is typically more sensitive. Frequency-domain specifications such as total harmonic distortion (THD), the spurious-free dynamic range (SFDR), or the signal-to-noise and distortion (SINAD) ratio characterize the presence of spurious signals on the $C_P(T)$ curve. An example of an extreme type of spurious signal, the missing codes effect, is shown in Fig. 7. It should be noted that spurious signals significantly increase when the signal amplitude approaches the ADC range limit.

We conclude that an ADC optimized for accurate dc and low-frequency ac measurements is more suitable as a ND-ADC, whereas an ADC optimized for precision ac-signal analysis or high-quality audio applications is more appropriate as the $\Delta V-$ADC. ADCs with nominal resolution not less than 16-bit and frequency band not less than from 0 to 25 kHz (which corresponds to 50 kHz and more of sampling and output frequency) are recommended. Low input impedance of the ADC provides shunting of the circuitry and decreases the accuracy of temperature measurements. We recommend input impedance greater than 1 MΩ. Note that only ADCs with true differential inputs can be used; those with pseudodifferential, single-ended or inputs polarized by any means require an additional preamplifier with differential inputs (an example is shown in Fig. 8). Inasmuch as a preamplifier is typically used for $\Delta V-$ADC, this requirement for $\Delta V-$ADC is not important.

Typically we use National Instruments NI5911 and Hewlett-Packard HP3458A as the $\Delta V-$ADC and Iotech DaqBoard/2005 and ADC488 as the ND-ADC.

E. Differential mode: Acquisition of differential voltage data

The initial ΔV-signal is amplified using a custommade, low-noise preamplifier with differential input and asymmetrical output. Then, the amplified signal is digitized by a precision ΔV-ADC. The principal circuitry of the preamplifier is demonstrated in Fig. 8. The preamplifier is designed using the classical scheme for an instrumentation amplifier.[10] The preamplifier is based on Linear Technology LT1028AC operational amplifiers with ultralow voltage and current spectral noise densities: $e_{V\text{opamp}}=0.85\ \text{nV}/\sqrt{\text{Hz}}$ and $e_{I\text{opamp}}=1.0\ \text{pA}/\sqrt{\text{Hz}}$, respectively (typical values, input referred, measured at 1 kHz frequency and ambient temperature of 25 °C), and good high-speed characteristics (typical gain–bandwidth GBW product value of $f_{\text{GBW}}=75\ \text{MHz}$).[11] The total input referred voltage noise density e_V of the preamplifier can be expressed as

$$e_V=\sqrt{2e_{V\text{opamp}}^2+2(e_{I\text{opamp}}R_{\Delta V})^2+e_{VT}^2}, \tag{20}$$

where the spectral density of thermal (Johnson) noise e_{VT} is given by

$$e_{VT}=\sqrt{4kTR_{\Delta V}}, \tag{21}$$

where k is the Boltzmann constant (1.38×10^{-23} J/K) and $R_{\Delta V}$ is the resistance of the source of the ΔV signal. Typical values of $T=300$ K and $R_{\Delta V}=200\ \Omega$ (for Pt metallization) give $e_{VT}=1.8\ \text{nV}/\sqrt{\text{Hz}}$, which is significantly larger than $e_{I\text{opamp}}R_{\Delta V}=0.2\ \text{nV}/\sqrt{\text{Hz}}$ and $e_{V\text{opamp}}$. So, in this case, the value of $e_V=2.2\ \text{nV}/\sqrt{\text{Hz}}$ is determined largely by e_{VT}. Modifications of the sensor design can considerably reduce the value of $R_{\Delta V}$. Replacing Pt metallization by a Au one decreases $R_{\Delta V}$ about fivefold; shortening the heater and increasing the thickness of the metallization will also reduce $R_{\Delta V}$. In this case the contribution of the $e_{V\text{opamp}}$ term will grow and, at some point, can be the major type of noise. Using n operational amplifiers ($n>1$) in parallel[11] can solve this problem. The effective voltage noise density e_V of such design will be reduced by a factor of $\sqrt{n}$. Current noise e_I will be increased by the same factor, but it will not increase the total noise because in Eq. (20) the term with the e_I value contains a reduced $R_{\Delta V}$ coefficient.

The gain of preamplifier g is a subject for special consideration. The output signal of the preamplifier is measured by an $\Delta V-$ADC, which is characterized by input referred voltage noise density $e_{V\text{ADC}}$. The $\Delta V-$ADC adds additional noise to the value measured unless the gain of the preamplifier is so high that $e_V\times|g|\gg e_{V\text{ADC}}$. On the other hand, the gain of the preamplifier is limited by the amplitude of the ΔV signal: after amplification this signal should not exceed the full scale input range of the $\Delta V-$ADC device. For example as shown in Fig. 4, the amplitude of the signal is ~80 mV, and for the typical input range of ±10 V the gain should not exceed 120.

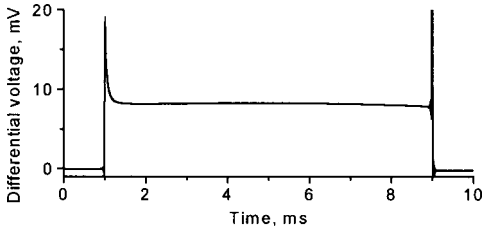

FIG. 9. Typical $\Delta V(t)$ dependence in an idle experiment. This measurement was made before the measurements shown in Fig. 4.

To keep the signal in the input range of the ADC without sacrificing signal-to-noise characteristics, several methods have been used. Using the ADCs with ultrahigh resolution gives the best results. An alternative is using a preamplifier with regulated gain. In this case, the low gain values can be used for massive samples with a high ΔV signal (when there is no increase in noise seen in the strong signal), while the high gain values can be useful for small samples. However, even in small sample and idle experiments, the ΔV signal can be high enough so as to limit the possible gain value due to nonideal matching of the sample and reference sensors. Figure 9 demonstrates a typical ΔV signal for the idle experiment. Although the ΔV signal shown in Fig. 9 is relatively small (~10 mV) because both sensors are match well, the gain would be limited to 1000 (10 V/10 mV) for a typical $\Delta V-$ADC input range of ±10 V. If we cared to measure the transient process at the beginning of the scan shown in Fig. 9 (at 1 ms), it would require gain less than 500 (10 V/20 mV).

To reject the strong ΔV signal caused by the difference in sensors, a special method can be used. As schematically illustrated in Fig. 10(a), a low gain preamplifier with gain g_1 is used to acquire data (low-gain baseline) from the first idle experiment. Then, in the additional idle experiment and during the experiment with the sample, the baseline is repeated by a function generator [a digital-to-analog converter (DAC)], and is subtracted from the signal by an additional operational amplifier. The result of the subtraction is additionally amplified (with gain g_2) and filtered. The total gain for the signal, measured by $\Delta V-$ADC, is equal to g_1g_2

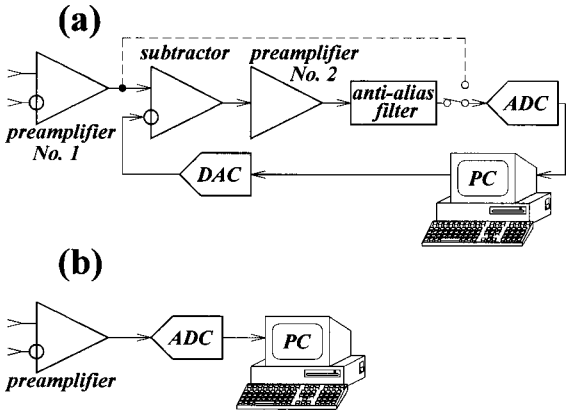

FIG. 10. (a) Block diagram of baseline signal subtraction for the high-gain ($g_1\times g_2$) method. The dashed line is used to acquire data in the first idle experiment. Then, in the second idle experiment and the experiment with the sample, the baseline accumulated is subtracted from the signal and the result is additionally amplified. (b) Block diagram of the regular (low-gain) method.

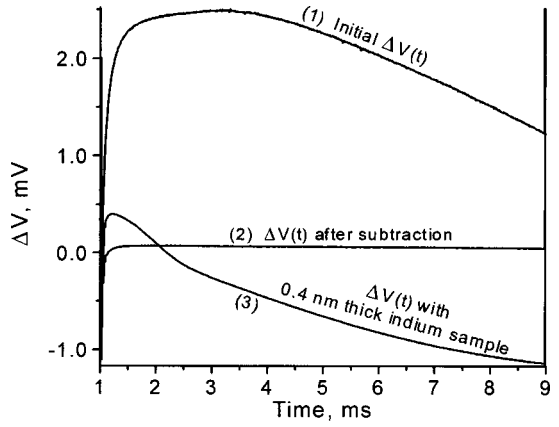

FIG. 11. ΔV data acquired in the baseline subtraction method. (1) Initial ΔV signal in the low-gain ($g_1=-28$) measurement (the first idle experiment). (2) High-gain ($g_1 g_2=704$) baseline acquired in the second idle experiment. (3) ΔV data acquired in the experiment with the sample (0.4 nm thick indium deposit). All curves are averages of 100 scans from room temperature up to about 300 °C.

(high-gain measurement). The additional idle experiment gives the baseline for the high-gain measurement. The sequence of data acquisition is illustrated in Fig. 11. The standard data acquisition circuitry is shown in Fig. 10(b) for comparison. Technically, repeatable generation of a low noise signal is easier than digitizing a signal with the same signal-to-noise ratio. For this scheme, illustrated in Fig. 10(a), we use a 12-bit Hewlett-Packard 33120A 15 MHz function/arbitrary wave form generator with a Hewlett-Packard HP3458A voltmeter as the ADC. An example of improvement in the data achieved by this method is shown in Fig. 12. Curve (1) obtained using high-gain measurement [Fig. 10(a)], is significantly less noisy than curve (2) obtained by low-gain measurement [Fig. 10(b)]. Note that the decreased noise level in the high-gain curve (1) allows us to resolve the fine structure of the melting peak (shown in Fig. 12 between 1.5 and 3 ms) of deposited indium clusters.[2]

F. Differential mode: Current source

The differential mode of TDSC sets special requirements on the noise level of the current source that feeds the heater

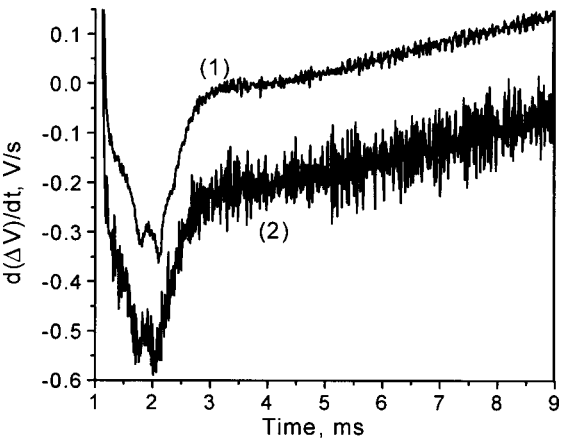

FIG. 12. (1) $d(\Delta V)/dt$ signal obtained in high-gain $g_1 g_2=704$ and (2) low-gain $g_1=-28$ measurement. Sample: 0.4 nm thick indium deposit. Curve (1) is shifted vertically for clarity. Both curves are averages of 100 scans from room temperature up to about 300 °C.

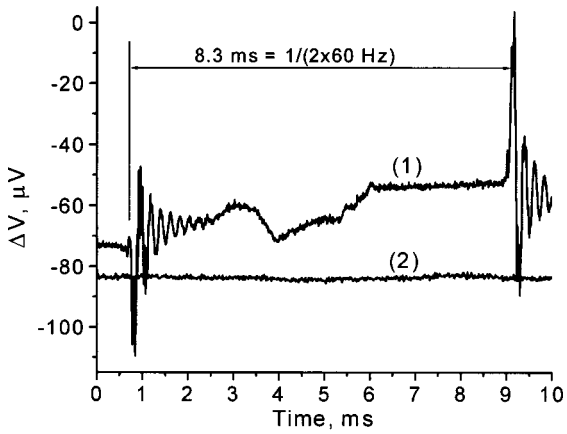

FIG. 13. (1) Spurious signals in the ΔV signal. For comparison (2) the same curve for decoupled current sources is presented. Both curves represent a single scan with no current through the sensors.

of the sensor. To get the best results, the voltage noise in the heater e_{VH} caused by noise of the current through the heater e_{IH}, should be much less than the thermal noise in the heater e_{VTH}. Here e_{VH}, e_{IH}, and e_{VTH} are spectral noise densities, $e_{VH}=R_S e_{IH}$, and $e_{VTH}=\sqrt{4kTR_S}$. Typical values of $T=300$ K and $R_S=70\ \Omega$ (for Pt metallization) give $e_{VTH}=1.1$ nV/$\sqrt{\text{Hz}}$, so e_{IH} should be much less than 16 pA/$\sqrt{\text{Hz}}$. In order to achieve this level of current noise, no active regulators of the current are used in the current source, as can be seen in Figs. 2 and 3. For typical values of $V_{SUP}=20$ V and $R_A=1\ \text{k}\Omega$, $e_{IH}=\sqrt{4kT/(R_A+R_S)}=3.9$ pA/$\sqrt{\text{Hz}}$. It is recommended that one use high quality components for the current source. We typically use low-noise stable wire-wound resistors (for example, Vishay Dale RS-2B),[12] and logic level *N*-channel enhancement-mode metal–oxide–semiconductor field-effect transistors (MOSFETs) with low resistance in the open state as switches (for example, the Fairchild Semiconductor RF1K490088,[13] with resistance at open state $R_{DS(\text{on})}=0.06\ \Omega$, or the RFP30N06LE, with $R_{DS(\text{on})}=0.047\ \Omega$).

Another important aspect of the design is that both current sources (for the sample and reference sensors) should be precisely ac and dc *decoupled*, both from each other and from laboratory power lines. The whole system should be grounded at one point (typically the middle of the connection between the low-potential probes of sensors, as shown in Fig. 3). Neglecting these requirements creates ground loops and introduces significant spurious signals. This effect is illustrated in Fig. 13, where the initial signal (curve 1) and the signal after decoupling of the current source from power lines (curve 2) are shown. Note that spurious signals caused by ground loops typically appear as periodic signals with frequency of ac power and its second harmonic (60 and 120 Hz, respectively, in the U.S.).

Decoupling the current sources can be done in different ways. We have used two different types of current source in order to decouple the sources from each other and from the laboratory power lines. The first is based on the use of (off-the-shelf) 9 V batteries and the second is based on use of high quality capacitors. We have found that the capacitor system is better due to its long-term stability as well as its excellent scan-to-scan reproducibility. Details of each type of

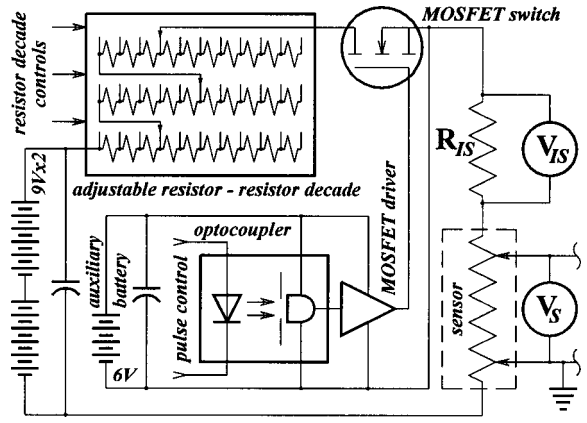

FIG. 14. Battery-based current source.

current source are now discussed. The most simple one is using batteries as a power supply. Figure 14 schematically illustrates this. The disadvantage of this method is that the discharge characteristics of batteries are not stable from scan to scan. Additionally, the voltage of the supplies should be monitored during the experiment to prevent failure caused by the limited electrical capacity of batteries. We have found that stability characteristics strongly depend on the type of battery used. We typically use Duracell 9 V PC1604 batteries with an alkaline $Zn-MnO_2$ electrochemical system, made in the U.S., and Ultralife 9 V U9VL batteries[14] with a $Li-MnO_2$ system, made in the U.S. Each current supply typically contains two batteries connected serially.

A more advanced current source exploits capacitors as a power storage medium instead of batteries. A capacitor-based battery replacement for the current supply is shown in Fig. 15. The capacitors are recharged before each scan by a dc power supply, fed by laboratory ac power lines. During the scan, the capacitors are disconnected from the dc power supply. Typically, discharge of the capacitors during the scan is less than 1%. For example, for 20 V of initial voltage, a typical assembly with 5000 μF of total capacity stores $20\ \mathrm{V}\times 5000\ \mu\mathrm{F}=0.1$ C of charge; the typical scan shown in Fig. 4 consumes about $18\ \mathrm{mA}\times 8\ \mathrm{ms}\approx 0.14$ mC. We typically use high-stability, high-frequency wet tantalum capacitors (for example, the Vishay Sprague 135D and M39006).[15]

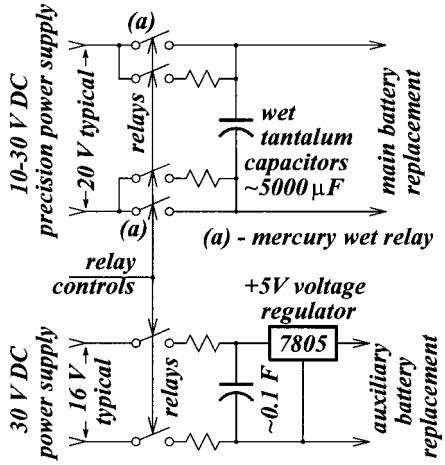

FIG. 15. Capacitor-based replacement for the battery-based current supply shown in Fig. 14.

Good ac decoupling can be achieved by minimizing parasitic electric capacitance between the current supply and all ac-fed, dc power supplies. Switches, which connect energy-accumulating capacitors and dc power supplies, should have negligible capacitance across an open connection. Electromechanical relays usually meet this requirement.

Since accumulating data from many scans is our usual practice, the repeatability of scans is important. Repeatability of the voltage across the energy-storing capacitors before each scan can be improved by using additional relays to charge the capacitor, as shown in Fig. 15. After being discharged in a scan, the capacitors are first recharged through a regular relay with high current capacity and a current-limiting resistor. After some time interval, a mercury wet relay makes an additional connection between the capacitor and the dc power supply. Mercury contacts provide negligible contact resistance even for small charge currents at the end of the charging procedure, and thus ensure repeatability of the voltage on the capacitor. Additionally, the dc power supply for charging the main energy-accumulating capacitor should be stable. We typically use a Hewlett-Packard E3632A dc power supply with output voltage stability of $\pm 0.02\%\ \pm 1$ mV.

G. Differential mode: Additional considerations

1. Heating rates: Hardware limitations

As mentioned above, the typical heating rates are between 15 and 200 K/ms. Experimentally, the heating rates are controlled either by adjusting the value of the resistor in the heater circuit (see Figs. 2, 3, and 14) or (more rarely) by adjusting the voltage of the current supply. The range of the heating rate is limited by two main factors. As the heating rate is lowered, heat loss to the surroundings increases and the system departs from the ideal adiabatic condition. In addition, at lower rates, the overall uniformity of the temperature deteriorates, especially at the edges of the cell. Although we can partially compensate for the heat loss,[9] correction for the temperature nonuniformity requires additional investigation. Consequently, to achieve adiabatic conditions with the present cell design, the heating rate should be significantly larger than the passive cooling rate of the cell, which is typically 1–2 K/ms in the 100–200 °C temperature range.

The upper limit of the heating rate is set by transient processes mostly at the start of a scan [for example, see Figs. 4(e), 9, 11, 12, 18]. These processes typically take a few tenths of a millisecond. To reduce transient processes, all of the equipment that is connected directly to the sensors (e.g., the current supply and ADCs), should be in close proximity and linked by short connecting wires.

Interestingly, the temperature lag effect typically is not a limiting factor for the upper value of the heating rates in the TDSC technique. The lag between the temperature of the thermometer and the average temperature of the sample is inherent for dynamic methods and is a common problem in conventional DSC.[16] Nevertheless, for typical samples used in TDSC measurements, the thickness does not exceed several hundred nanometers and the temperature gradient across

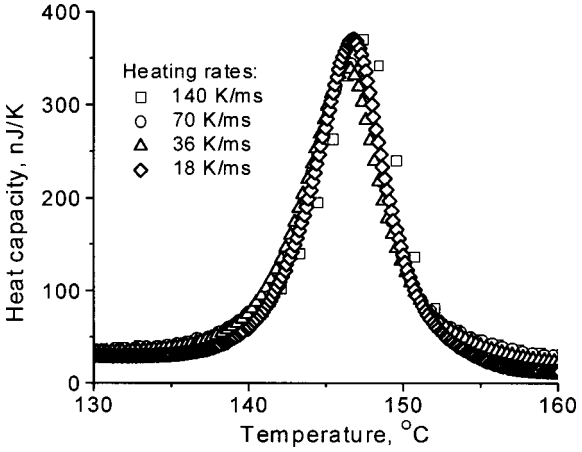

FIG. 16. Heat capacity of a 5 nm thick indium film. The curves were collected at different heating rates. Each curve is an average of 100 scans. Only the temperature range near the melting peak is shown.

the sample–membrane–heater ''sandwich'' is negligible. The lag in temperature can be estimated using the following heat transfer considerations. An insulated thick plate with thickness h is suddenly exposed to constant heat input q on the front side of the plate. Above Fourier number $F_0=\sigma t/\rho c h^2=0.5$ the drop in temperature ΔT across the plate is constant, $\Delta T=qh/2\sigma$, where σ is the thermal conductivity of the plate.[17] Noting that $q=\rho c h dT/dt$ and using the characteristic thermal diffusion (TD) time $\tau_{TD}=h^2\rho c/\sigma$, one can express $\Delta T=(\tau_{\mathrm{TD}}/2)(dT/dt)$ and $F_0=t/\tau_{\mathrm{TD}}$. One of the worst cases of samples, investigated by the TDSC method, was a 400 nm thick polystyrene film.[5] Using $\rho=1.043\ \mathrm{g/cm^3}$,[18] $c=1.223\ \mathrm{J\,g^{-1}\,K^{-1}}$, and $\sigma=0.105\ \mathrm{W\,m^{-1}\,K^{-1}}$, the $\tau_{\mathrm{TD}}\approx 2\ \mu$s. This means that, after about 1 μs, the difference in temperature across the sample is about 0.2 K even at the highest heating rate of 200 K/ms used. Note that, using typical ADCs with a 100 ksample/s sampling rate, there is 2 K resolution at the same heating rate, which is much larger than ΔT. So, even for this extreme case the lag in temperature is negligible. Nevertheless, it is good practice to test the system being investigated for thermal conductivity problems, when possible. This can usually be done using different heating rates.[16] Thermal processes in the sample used for this test should exhibit no inherent dependence on the heating rate (melting of crystals, etc.). For example, Fig. 16 demonstrates the absence of the thermal lag effect in a 5 nm thick discontinuous In film. The shift of the melting peak is comparable to the temperature resolution of the measurement (the distance between experimental points).

2. Real-time control and time reproducibility

The TDSC equipment in differential mode requires synchronization between events such as the start and finish of current pulses through the sensors, the timing of charge capacitors, and the triggering of measurement devices. Good synchronization and repeatability of all time intervals are achieved by using a simple, microcontroller-based control device, e.g., a pattern generator (PG), as illustrated in Fig. 17. The PG acquires the time schedule for the experiment from the computer and then controls the measurement process in real time. Clocking of the PG is based on a standard quartz resonator, which provides excellent frequency stability (± 50 ppm maximum for the currently used 8 MHz HC-49U crystal[19]).

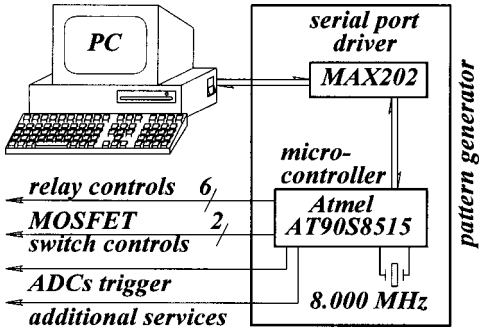

FIG. 17. Real-time control system.

Good synchronization of current pulses also requires fast MOSFET switches and their control circuitry. Ac and dc decoupling of the MOSFET control circuitry from the PG output is achieved by a high speed optocoupler (see Fig. 14). We typically use Hewlett-Packard HCPL-2400 optocouplers[20] with a 40 MBd typical data rate. The MOSFET driver should generate high current pulses to speed up switching of the MOSFET transistor, but should not consume significant current from the power supply, which has a limited capacity for stored energy. We typically use complementary MOS (CMOS) drivers with high output currents (six Schmitt-trigger inverters, SN74ACT14N,[21] with ± 24 mA output current for each element and 1.5 mA maximal supply current).

Since the typical time interval between consecutive scans is 1 s, the operation time t_o of all electromechanical relays in the system should be much less than 1 s. We use miniature relays with a few milliseconds operation time t_o [Tyco V23026,[22] $t_o=2$ ms, SRC Devices LQ52,[23] $t_o=6$ ms]. The maximum value of t_o for the mercury wet relays[24] is 1.75 ms.

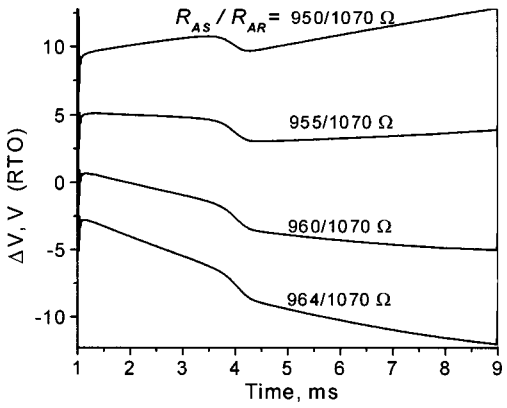

FIG. 18. Illustration of the sensitivity of the differential voltage [referred to the output (RTO) of the preamplifier] to changes in values of adjustable resistors R_{AS} and R_{AR} (see Fig. 3). The preamplifier gain is equal to 704. Each curve is an average of 100 scans from room temperature up to about 300 °C. Sample: 2 nm thick indium film (the step in each curve shows melting of the indium particles).

3. Heater circuit adjustment

There is some degree of freedom in adjustment of the sensor's heater circuitry. Generally, the first step in a typical experiment is to establish a nominal heating rate. This is easily accomplished by coarse adjustment of the trimming resistors, R_{AR} and R_{AS} (see Fig. 2). If the instrument is to be used in differential mode, which has the potential for high sensitivity, the response of both heaters must be carefully matched on a very fine scale. This can be accomplished by adjusting resistor R_{AS} and thus fine-tuning the ratio R_{AS}/R_{AR}. Even small changes in this ratio will produce significant changes in the $\Delta V(t)$ signal, as shown in Fig. 18.

Adjusting the circuitry to obtain a flat $\Delta V(t)$ (as horizontal as possible, like the second curve from the top in Fig. 18) suppresses noise. There are several possible reasons for this effect. During data processing, the noisy terms contained in the $d(\Delta V)/dt$ factor are weighted less than other, less noisy terms. From a hardware point of view, a $\Delta V(t)$ signal that spans a small range collects fewer spurious signals. Full scale signals are generally more affected by integral nonlinearity in an ADC transfer function. Moreover, an ADC transfer function may exhibit more errors upon an increase in $d(\Delta V)/dt$. Additionally, making the $\Delta V(t)$ signal flatter sometimes allows us to reduce the range of the ADC, which often gives an advantage in decreasing the noise level.

Adjustments in the trimming resistors in order to obtain a flat $\Delta V(t)$ are recommended for the idle experiment in all cases. However, care should be taken if adjustments are performed in subsequent experiments with the sample. Only adjustment of the sample circuitry (e.g., of R_{AS}) is allowed. It is imperative that the reference circuitry (e.g., R_{AR}) remains the same for both the idle and subsequent experiments, in order to use corrections derived from the idle experiment.[9] Additionally, after adjustment of R_{AS} in the experiment with the sample, no simplified methods of calculation[9] can be used.

It is important to be able to reproducibly set and reset the resistance in the heater circuit many times over the course of the experiment. An idle experiment typically includes many scans with different heating rates and, consequently, different settings for the adjustable resistors. In subsequent experiments with the samples, these resistor values, at least for the reference part of circuit, should be precisely reset to the original values. Because of this, the use of a precision resistor decade as an adjustable resistor is strongly recommended. Trimming of the adjustable resistors can be made either manually or (preferably) electronically. In the latter case, effective ac and dc decoupling of the decade from the control device (see the discussion in Sec. III E) should be made. We control the decades by electromechanical relays (typically by the Tyco V23026).[22]

There are concerns about choosing the resistance value of current measurement resistors R_{IS} and R_{IR} (Fig. 3). As mentioned in Sec. III A, increasing the R_{IS} and R_{IR} values suppresses noise, but there are limits to these resistances.

Analog common inputs of all ADCs (or preamplifiers) should be connected to the ground terminal, shown in Fig. 3, to prevent excessive noise. Increasing R_{IS} and R_{IR} increases V_{IS} and V_{IR} values. The top inputs of the V_{IS} and V_{IR} voltmeters (as they appear in Fig. 3) have the highest common-mode potential (voltage between analog common and given inputs). Typically, the common-mode potential should not exceed 12–15 V (even if the voltage between signal inputs is within the voltmeter range limits). Exceeding the common-mode potential can cause faulty measurements, parasitic current through the input to the analog ground and, ultimately, permanent ADC failure. Even within the range specified by the manufacturer, measurements close to the limit of the common-mode potential can introduce additional spurious signals. As a rule of thumb, the voltage between the analog ground and any ADC (or preamplifier) input should be kept below 10 V all the time.

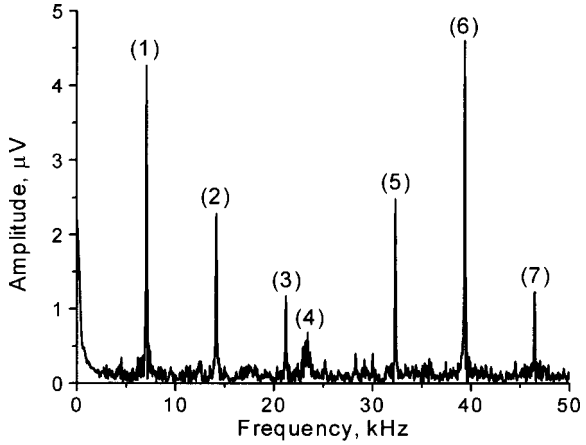

FIG. 19. Spectral components of high frequency noise in the ΔV signal (FFT plot). Components (1)–(3) and (5)–(7) are caused by the CRT monitor, and (4) is caused by the on-line UPS.

Additionally, large R_{IS} and R_{IR} reduce the ability to manipulate the heating rate by adjusting R_{AS} and R_{AR}.

The voltage of the current supply is set to the highest possible level in order to minimize noise and changes in current during the scan, and is rarely adjusted.

4. Grounding considerations

As shown above, ground loops created by coupled current supplies introduce intolerable noise in the ΔV data. This clearly demonstrates that proper grounding, as well as shielding, is a critical part of TDSC equipment design. Common terminals of the analog part of all ADCs (and preamplifiers) should be connected to one point, which is typically the middle of the connection between low-potential probes of sensors, as shown in Fig. 3. All ground connections should be made with short, thick, copper, insulated wires. All signal connectors should be as short as possible and should have a grounded shield. Shielded twisted pairs are recommended. The vacuum chamber for TDSC should be metallic or surrounded by metal, and all metal parts should be grounded.

5. Additional noise sources

Noisy equipment in or near the laboratory can cause serious problems. Vacuum chambers are typically equipped with voltage regulators for different purposes (for example, resistive heating for *in situ* deposition). These usually use solid-state regulators and are noisy. Generally, all impulse

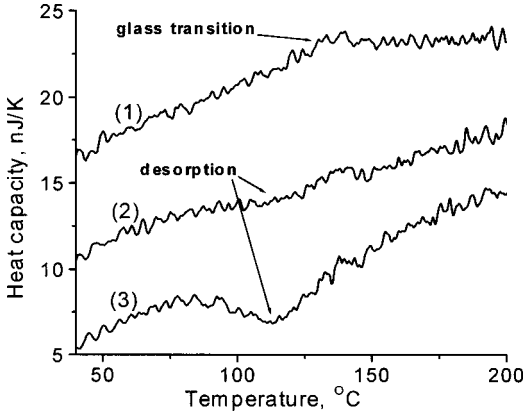

FIG. 20. Illustration of spurious signals due to gas adsorption to the reference sensor for differential heat capacity measurements of 1.5 nm thick spin-cast polystyrene film after 60 s annealing at 140 °C. Each curve represents one scan. (1) The pressure is 2×10^{-8} Torr, and the reference sensor is prepulsed/heated. (2) The same vacuum, with no prepulsing/heating. (3) The pressure is 2×10^{-7} Torr, with no prepulsing/heating. The endothermic desorption process from the reference sensor (which looks like an *exothermic* process in the film investigated) masks the glass transition in (2) and (3). The curves offset for clarity.

power devices are inherently noisy. For instance, by switching an on-line uninterruptable power supply (UPS) to bypass mode and replacing regular cathode ray tube (CRT) computer monitors by liquid crystal displays (LCDs) we can reduce the noise significantly. Figure 19 demonstrates a typical fast Fourier transform (FFT) plot for the ΔV signal acquired by the setup equipped with a UPS and CRT monitor. Spectral components of the high frequency noise are caused by the CRT monitor [components (1)–(3) and (5)–(7)] and by the UPS [component (4)] shown in Fig. 19. Nevertheless, we have found that modern switching-mode low-power supplies (such as computer power supplies) do not introduce noticeable noise.

6. Vacuum-dependent spurious signals

Adsorption and desorption of contaminants (e.g., adsorbed gases) in poor vacuum can generate significant spurious signals for small sample experiments, as illustrated in Fig. 20. Preheating the sensors by an additional scan immediately before measurement usually reduces this problem. Nevertheless, in some cases, preheating the sensor with the sample is not possible. This could be the case if the sample were prepared a by special treatment, and the experiment probes the state of the sample right after this treatment. Probing the heat capacity of a freshly annealed polymer film is one example.[5] The preheating scan would destroy the state of the film. In such cases, improving vacuum conditions is recommended. Additionally, preheating/pulsing the reference sensor is useful.

ACKNOWLEDGMENTS

This work was supported by National Science Foundation Grant No. DMR 0108694 and by American Chemical Society Petroleum Research Fund Grant No. 33580-AC7.

NOMENCLATURE

Variable (parameter)	Definition
C_P	heat capacity (J/K)
C_P^{cell}	heat capacity of empty cell (J/K)
C_P^{SMP}	heat capacity of the sample (J/K)
c	specific heat capacity ($\text{J kg}^{-1}\text{K}^{-1}$)
c_{Me}	specific heat capacity of the metallization ($\text{J kg}^{-1}\text{K}^{-1}$)
c_{SiN}	specific heat capacity of the SiN_x membrane ($\text{J kg}^{-1}\text{K}^{-1}$)
c_{SMP}	specific heat capacity of the sample ($\text{J kg}^{-1}\text{K}^{-1}$)
e_I	input referred current spectral noise density ($\text{A}/\sqrt{\text{Hz}}$)
e_{IH}	spectral noise density of current through the heater ($\text{A}/\sqrt{\text{Hz}}$)
$e_{I\text{opamp}}$	input referred current spectral noise density of an operational amplifier ($\text{A}/\sqrt{\text{Hz}}$)
e_V	input referred voltage spectral noise density ($\text{V}/\sqrt{\text{Hz}}$)
$e_{V\text{ADC}}$	input referred voltage spectral noise density of an ADC ($\text{V}/\sqrt{\text{Hz}}$)
e_{VH}	spectral noise density of voltage across the heater ($\text{V}/\sqrt{\text{Hz}}$)
$e_{V\text{opamp}}$	input referred voltage spectral noise density of an operational amplifier ($\text{V}/\sqrt{\text{Hz}}$)
e_{VT}	thermal (Johnson) spectral noise density ($\text{V}/\sqrt{\text{Hz}}$)
e_{VTH}	thermal (Johnson) spectral noise density in the heater ($\text{V}/\sqrt{\text{Hz}}$)
F_0	Fourier number
f_S	sampling frequency (Hz)
f_{GBW}	gain–bandwidth product (Hz)
g, g_1, g_2	gain of the preamplifier
h	thickness (m)
h_{Me}	thickness of the metallization (m)
h_{SiN}	thickness of the SiN_x membrane (m)
h_{SMP}	thickness of the sample (m)
I	current (A)
I_S	current through the sample cell heater (A)
I_R	current through the reference cell heater (A)
k	Boltzmann constant (1.38×10^{23} J/K)
l	distance between two voltage probes (m)
N	number of scans
n	number of operational amplifiers in the parallel design
P	power (W)
q	heat input (W/m^2)
R	resistance (Ω)
R_S	resistance of the sample cell heater (Ω)
R_R	resistance of the reference cell heater (Ω)
R_{ADJ}	resistance of the adjustment resistor (Ω)
R_{AS}	resistance of the adjustment resistor in the sample cell circuit (Ω)
R_{AR}	resistance of the adjustment resistor in the reference cell circuit (Ω)

R_{IS} resistance of the current measurement resistor in the sample cell circuit (Ω)
R_{IR} resistance of the current measurement resistor in the reference cell circuit (Ω)
$R_{DS(\mathrm{on})}$ resistance of the MOSFET switch in the open state (Ω)
$R_{\Delta V}$ resistance of the source of ΔV (Ω)
r_T temperature resolution (K)
T temperature (K, °C)
ΔT drop in temperature across the plate (K)
t time (s)
t_o relay operation time (s)
V voltage (V)
V_S voltage across the sample cell heater (V)
V_R voltage across the reference cell heater (V)
V_i, V_{i+1} consecutive results of voltage measurement (V)
V_{IS} voltage across the current measurement resistor in the sample cell circuit (V)
V_{IR} voltage across the current measurement resistor in the reference cell circuit (V)
V_{SUP} voltage of power supply (V)
w width of the heater strip (m)
α temperature coefficient of resistivity (K^{-1})
α_R temperature coefficient of resistivity of the reference cell heater (K^{-1})
Δt time between two consecutive measurements (samples) (s)
ΔV differential voltage (V)
δ_{Cp} fractional error of C_P
$\delta_{Cp\mathrm{SMP}}$ fractional error of C_P^{SMP} obtained by the differential method
$\delta_{Cp\mathrm{SMP}}^{\mathrm{dif}}$ fractional error of C_P^{SMP} obtained by the differential method
$\delta_{Cp\mathrm{SMP}}^{\mathrm{nondif}}$ fractional error of C_P^{SMP} obtained by the non differential method
$\delta_{dT/dt}$ fractional error of dT/dt
δ_{VS} fractional error of V_S
δ_{VIS} fractional error of V_{IS}
$\varepsilon_{dT/dt}$ rms error (noise) of dT/dt (K/s)
ε_T rms error (noise) of T (K)
ε_V rms voltage error (noise) (V)
ε_{VS} rms error (noise) of V_S (V)
ε_{VIS} rms error (noise) of V_{IS} (V)
$\varepsilon_{\Delta V}$ rms error (noise) of ΔV (V)
σ thermal conductivity ($\mathrm{W\,m^{-1}\,K^{-1}}$)
ρ specific density ($\mathrm{kg/m^3}$)
ρ_{Me} specific density of the metallization ($\mathrm{kg/m^3}$)
ρ_{SiN} specific density of the SiN_x membrane ($\mathrm{kg/m^3}$)
ρ_{SMP} specific density of the sample $\mathrm{kg/m^3}$
τ_{TD} characteristic thermal diffusion time (s)

[1] S. L. Lai, J. Y. Guo, V. Petrova, G. Ramanath, and L. H. Allen, Phys. Rev. Lett. **77**, 99 (1996).
[2] M. Yu. Efremov, F. Schiettekatte, M. Zhang, E. A. Olson, A. T. Kwan, R. S. Berry, and L. H. Allen, Phys. Rev. Lett. **85**, 3560 (2000).
[3] M. Zhang, M. Yu. Efremov, E. A. Olson, Z. S. Zhang, and L. H. Allen, Appl. Phys. Lett. **81**, 3801 (2002).
[4] A. T. Kwan, M. Yu. Efremov, E. A. Olson, F. Schiettekatte, M. Zhang, P. H. Geil, and L. H. Allen, J. Polym. Sci., Part B: Polym. Phys. **39**, 1237 (2001).
[5] M. Yu. Efremov, J. T. Warren, E. A. Olson, M. Zhang, A. T. Kwan, and L. H. Allen, Macromolecules **35**, 1481 (2002); M. Yu. Efremov, E. A. Olson, M. Zhang, Z. S. Zhang, and L. H. Allen, Phys. Rev. Lett. **91**, 085703 (2003).
[6] W. Winter and G. W. H. Hohne, Thermochim. Acta **403**, 43 (2003).
[7] S. A. Adamovsky, A. A. Minakov, and C. Schick, Thermochim. Acta **403**, 55 (2003).
[8] E. A. Olson, M. Yu. Efremov, M. Zhang, Z. S. Zhang, and L. H. Allen, J. Microelectromech. Syst. **12**, 355 (2003); D. W. Denlinger, E. N. Abarra, K. Allen, P. W. Rooney, M. T. Messer, S. K. Watson, and F. Hellman, Rev. Sci. Instrum. **65**, 946 (1994).
[9] M. Yu. Efremov, E. A. Olson, M. Zhang, S. L. Lai, F. Schiettekatte, Z. S. Zhang, and L. H. Allen, Thermochim. Acta (in press).
[10] J. Dostál, *Operational Amplifiers* (Elsevier Scientific, Amsterdam, 1981).
[11] Linear Technology LT1028/LT1128 ultralow noise precision high speed op amps datasheet; http://www.linear.com/pdf/1028fa.pdf.
[12] Vishay Dale RS, NS wirewound resistors, Document No. 30204; http://www.vishay.com/docs/30204/rsns.pdf.
[13] Fairchild Semiconductor Corp. RF1K49088 data sheet; http://www.fairchildsemi.com/ds/RF/RF1K49088.pdf; RFP30N06LE, RF1S30N06LESM data sheet, http://www.fairchildsemi.com/ds/RF/RFP30N06LE.pdf.
[14] Ultralife Batteries Inc., http://www.ulbi.com/techsheets/UBI-3001a-U9VL.pdf.
[15] Vishay Sprague model 135D wet tantalum capacitors, Document No. 40024; http://www.vishay.com/docs/40024/135d.pdf; M39006/09/21/22/25/30/31 wet tantalum capacitors, Document No. 40022; http://www.vishay.com/docs/40022/m39006.pdf.
[16] V. P. Kolesov, *Basics for Thermochemistry* (Moscow University Press, Moscow, 1996).
[17] *Handbook of Heat Transfer*, edited by W. M. Rohsenow and J. P. Hartnett (McGraw–Hill, New York, 1973).
[18] *Physical Properties of Polymers Handbook*, edited by J. E. Mark (American Institute of Physics, Woodbury, NY, 1996).
[19] ESC Inc., International, HC-49U quartz crystal data sheet; http://www.ecsxtal.com/pdf2/HC49U.PDF.
[20] Agilent Technologies, HCPL-2400, HCPL-2430 technical data; http://literature.agilent.com/litweb/pdf/5965-3586E.pdf.
[21] Texas Instruments, SN54ACT14, SN74ACT14 hex Schmitt-trigger inverter; http://www-s.ti.com/sc/ds/sn74act14.pdf.
[22] Tyco Electronics, V23026 series miniature, sealed PC board relay; http://relays.tycoelectronics.com/datasheets/PC_Board_Relays/V23026DS.pdf.
[23] SRC Devices, EMR series reed relays LM, LX, LQ; http://www.srcdevices.com/pdf/EMR_src2.pdf.
[24] SRC Devices, DIP 14 series reed relays MSS2, MSS&, PRMA, DSS7, PRME, MVS2, MVS7; http://www.srcdevices.com/pdf/dip14ser_src1.pdf.